CHAPTER – 6

Effect of doping metal ions on microstructural evolution and dielectric behaviors of $CaCu_3Ti_4O_{12}$ ceramics synthesized by semi-wet route

6.1 Introduction

Due to their significance and potential impact in a ceramic condenser, microwave device applications, and other electronic devices [1, 2], the ABO_3 (A and B cations of dissimilar sizes (B is less than A) and O is the anion) type of ceramic peroxides have attracted more in recent decades. Compared to traditional ferroelectric materials, the $CaCu_3Ti_4O_{12}$ (CCTO), which belongs to the ABO_3 family with a large dielectric constant, is the best choice (around 10^4-10^6). The calcium copper titanate (CCTO) has a cubic structure containing space group Im3 and the parameter for the lattices is 7.391 A^o [2, 3]. The dielectric behavior of CCTO peroxide has been refined by the different cationic substitutions as well as doping at Cu and Ti sites [4, 5]. By controlling the chemistry and microstructure of grain boundaries, cationic substitutions in CCTO directly affect the dielectric function, tangent loss, and electrical behavior. There are two forms of doping or replacement: both acceptor and donor. The accepter cationic substitutions are described as cations (Cu-site) with ionic charges lower than the ions they replace. The donor cationic substitutions are explained as cations with a higher ionic charge than the ions they replace, causing vacancies in the donor substituent CCTO perovskite structures [5, 7]. In complex perovskite structure, the acceptor doping metal ions are generally applied at B-site or Ti-site. Mn^{2+}, Mn^{3+}, Co^{2+}, Co^{3+}, Fe^{2+}, Fe^{3+}, Ni^{2+} and Zn^{2+} are some example of acceptor dopant. Acceptor dopants like Mn^{3+} on the Ti^{4+} site provide oxygen vacancy but without the liberation of an electron. In some literatures were found element containing 5+ or 6+ like as Nb^{5+}, Ta^{5+} and Sb^{5+} W^{6+} at B-sites (Ti-site) and some elements charge of 3+ like as La^{3+}, Bi^{3+} and Nd^{3+} are usually used in A-site (Ca-site) in CCTO perovskite [8].

The dielectric behavior of CCTO is also directly depending on the processing situation such as synthesized routes [3, 9] sintering temperatures[10] and sintering durations[11], a Synthesis route of $CaCu_3Ti_4O_{12}$ has played an important role in confirming the microstructural, and dielectrical behaviors. In the case of Mn and Fe substituted CCTO [12], these two dopants (metal ions) can cause exceptionally major changes in dielectrical behavior grains and grains boundaries. On the other hand, a remarkable decrease in dielectric constant in these two ceramic systems is still recognized for changes in grain boundaries electrical properties [13]. In recent times, numerous papers describing Y, Zr, and Ta substituted CCTO ceramics have been published. But the results of in these papers are completely different [14, 15]. The CCTO ceramics were synthesized by the use of metal nitrate at high temperatures using a solid-state method. Long reaction time, high calcination, and sintering temperature have been required for this process. Alternatively, during synthesis [16-18] some extra minor secondary phases (CuO, TiO_2, and Cu_2TiO_3) may also come out. On the other hand, the CCTO has also been prepared by a chemical process such as sol-gel using metal alkoxide which gives intimate and uniform metal ion mixing in the stoichiometric ratio. Titanium isopropoxide $Ti(OR)_4$ is very expensive in this route. So, we have synthesized Mn, Nb, and W doped CCTO through a semi-wet route sintered at 950^{o}C, 1050^{o}C, and 1100^{o}C, for 8 h, respectively and their comparative studies of morphology and dielectric behaviors. This procedure has the advantage of improving dielectric constant, dielectric loss, and microstructures of Mn, Nb, and W doped CCTO ceramic.

6.2. Experimental

6.2.1 Materials synthesis

The semi-wet method was used to synthesize the $CaCu_3Ti_{3.5}X_{0.5}O_{12}$ (X= Mn, W, and Nb). Chemicals calcium nitrate, $Ca(NO_3)_2.4H_2O$ (98% Merck, India), copper nitrate, $Cu(NO_3)_2.3H_2O$ (99% Merck, India), manganese acetate, $Mn(CH_3COO)_2.4H_2O$ (99% Merck, India), WO_2 (99% Merck, India), Nb_2O_5 (99% Merck, India) and titanium oxide, TiO_2 (99% Merck, India), were taken stoichiometrically in the molar ratio. Using distilled water was prepared a solution of $Ca(NO_3)_2.4H_2O$, $Cu(NO_3)_2.3H_2O$, and $Mn(CH_3COO)_2.4H_2O$. In a beaker, all solutions were mixed and solid TiO_2 was added in solution. In distilled water, the calculated amount of citric acid (99.5 %, Merck India) equivalent to metal ions was dissolved and mixed with the solution. The resulting solution has been heated to evaporate water on a 60-70^oC hot-plate magnetic stirrer and allows for self-ignition. After the removal of a lot of gases, a residual mass of CCTXO (X= Mn, Nb, and W) powders was obtained. Citric acid used in the ignition step as a complex agent that acts as a fuel. The resultant CCTXO powder was ground to obtain a fine powder by using agate and mortar. The powder was calcined at 850^oC for 6 h. All different calcined powder was used to make for cylindrical pellets with the use of 4 % Pollyvinylalcohol as a binder on applying 5 tons of pressure using hydraulic pressure for 120 seconds. At last, the CCTMO, CCTWO and CCTNO pellets were sintered at 950^oC, 1050^oC, and 1100^oC, for 8 h.

6.2.2 Characterization

An X-ray diffractometer (Rigaku miniflex 600, Japan) applying Cu-kα radiation with wavelength 1.5418 A^{o} was confirmed for the phase of $CaCu_3Ti_{3.5}X_{0.5}O_{12}$ (CCTXO) (X=Mn, W and Nb) ceramic sintered samples. Scanning electron microscope (ZEISS; model EVO18 research, Germany) attached with an energy-dispersive X-ray (EDX) (Oxford instrument, USA) analyzer confirmed the microstructure, as well as the elemental composition. A transmission electron microscope (TEM, Technai G2 20 S-Twin), analyzed the particle size. The samples were distributed in ethanol for TEM analysis, and 2 h sonicated. This suspension was deposited on a carbon-coated copper grid and dried in oven 8 h. LCR meter (PSM1735, NumetriQN4L, U.K.) has tested the dielectric details of silver-coated cylindrical pellets. The XPS investigation was conducted by using Thermo Fisher Scientific Kα (Waltham, MA) in broad scan survey mode and high energy resolution with AlK_{α} (1486.6 eV).

6.3. Results and discussions

6.3.1 X-ray diffraction studies

Fig. 6.1 presents the X-ray diffraction pattern of sintered $CaCu_3Ti_{3.5}X_{0.5}O_{12}$ (X= Mn, W, and Nb) (CCTXO) with a different dopant. It confirms the presence of CCTO as a major phase along with the lesser phase of TiO_2. XRD peak is exactly matched to JCPDS (card no.21-0140), reported the CCTO as the main phase along with TiO_2 minor secondary phase with JCPDS (card no.46-1238) [2, 18, 19, 31]. The crystalline size (D) of CCTXO (X=Mn, W, and Nb) was evaluated by using the Debye Scherrer formula.

$$D = K\lambda/\beta COS\theta \qquad (1)$$

where D is crystalline size, k is constant equal to 0.89, λ is a wavelength of X-ray, θ is the Bragg diffraction angle and β is the full width at half maximum (FWHM) in radians. The line broadening due to instrument effect eliminated by using a standard sample for XRD data to calculate the correct value of the crystalline sizes. The average crystallite size of CCTMO, CCTWO, and CCTNO was calculated 38.97 ± 10 nm, 56.23 ± 10 nm, and 42.41 ± 10 nm, respectively.

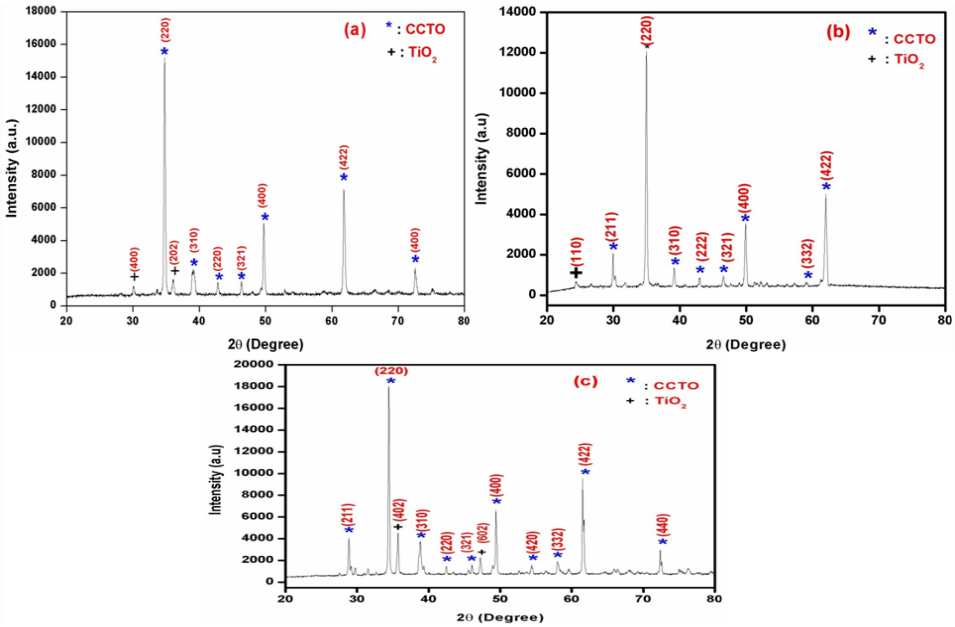

Fig. 6.1. XRD patterns of $CaCu_3Ti_{3.5}X_{0.5}O_{12}$ (a) X= Mn (b) X= Nb (c) X= W sintered at at 1223 K, 1323 K and 1373 K, respectively for 8 h.

6.3.2. Microstructural studies

Fig. 6.2 displays the bright-field TEM images (a, c and e) and their respective selected area diffraction pattern (SEAD) (b, d, and f) of sintered $CaCu_3Ti_{3.5}X_{0.5}O_{12}$ (X= Mn, Nb, and W) (CCTXO) with the different dopant. The observed particles size of CCTMO, CCTNO as well as CCTWO calculated by TEM was found to be 44 nm, 101 nm, and 51

nm, respectively. Figures 6.2(b, d, and f) show the SEAD pattern with single-crystalline in nature which confirms by the free-standing crystal [18, 20].

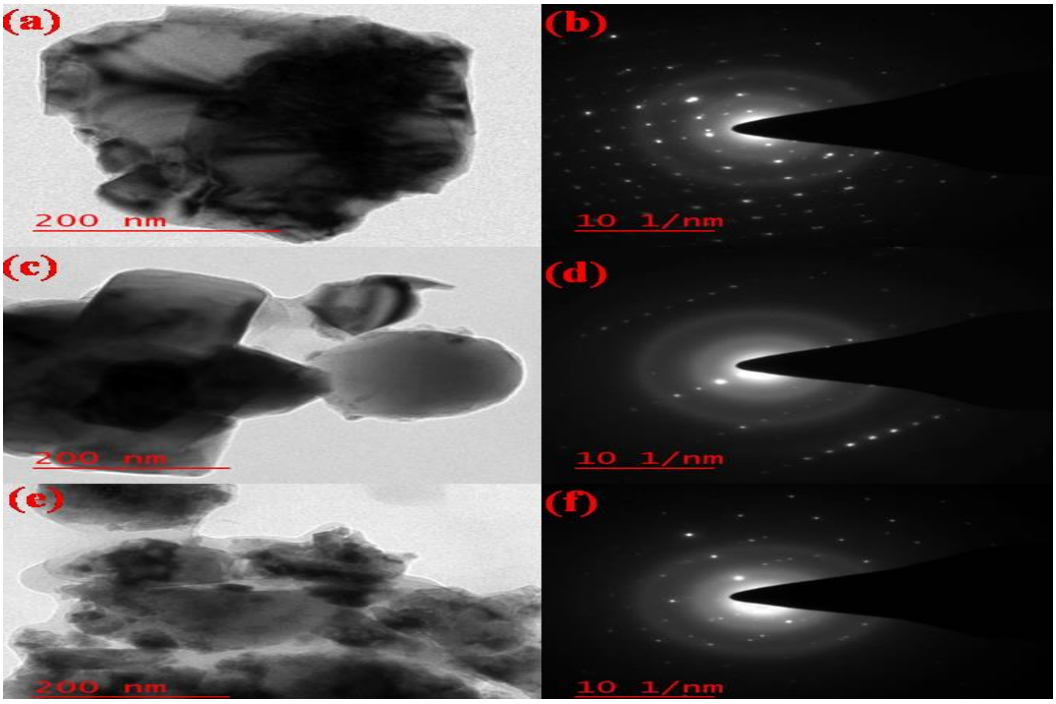

Fig. 6.2. Bright-field TEM images and their corresponding SEAD patterns of $CaCu_3Ti_{3.5}X_{0.5}O_{12}$ ceramics (a-b) X= Mn (c-d) X= Nb (e-f) X= W (Mn, Nb and W) sintered at 1223 K, 1323 K and 1373 K, respectively for 8 h.

Fig. 6.3(a-c) illustrates the SEM micrograph of CCTMO, CCTNO, and CCTWO samples, respectively. The doping of different metal ion directly affects the microstructure [18,21-24,31].CCTMO, CCTNO and CCTWO average grain size are 1.57 μm, 1.47 μm, and 1. 16 μm, respectively. The grain size directly depends on the doped or substituted metal ion. Figure 3(d-f) shows the CCTMO, CCTNO, and CCTWO energy-dispersive X-spectra (EDX) ceramics, which confirms the presence of Ca, Cu, Ti, Mn, Nb, W and O elements. Table 6.1 shows the atomic percentage of Ca, Cu, Mn, Nb, W and Ti, and

O elements with different metal ions which confirm the stoichiometry and purity of CCTMO, CCTNO, and CCTWO, respectively, ceramic materials.

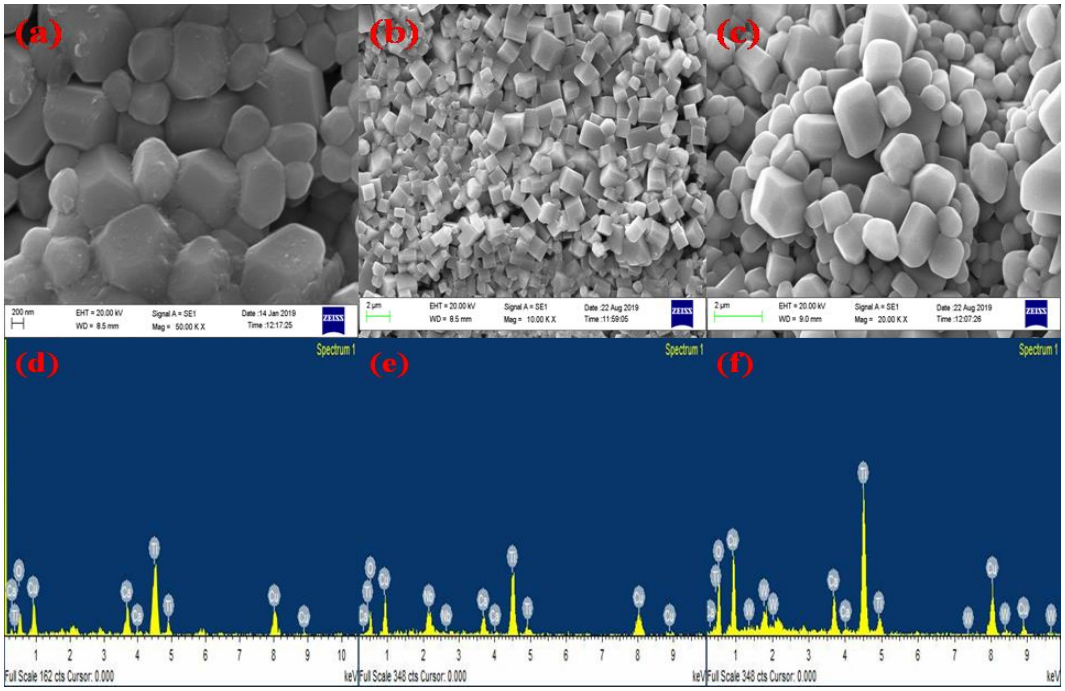

Fig. 6.3. SEM micrograph of $CaCu_3Ti_{3.5}X_{0.5}O_{12}$ ceramics (a) X= Mn (b) X= Nb (c) X= W and EDX spectra of $CaCu_3Ti_{3.5}X_{0.5}O_{12}$ ceramics (d) X= Mn (e) X= Nb (f) X= W sintered at 1223 K 1323 K and 1373 K, respectively for 8 h.

Fig. 6.4(a) presents the XPS spectrum in Mn 2p core levels for CCTMO samples sintered at 950ºC for 8 h. The highest peak at 643, 648, and 653 eV that against Mn $2p_{3/2}$ and Mn $2p_{1/2,}$ respectively shown in figure 4(a). The splitting of peak Mn 2p into Mn $2p_{3/2}$ and Mn $2p_{1/2}$ occur due to the spin-spin orbital coupling. The shoulder occurred at higher energy is show along the broadness of the peak for Mn $2p_{3/2}$ and Mn $2p_{1/2}$ as indicated by arrows which means that there are contributions from the mixed valent state of Mn ions. Due to this reason, Mn $2p_{3/2}$ and Mn $2p_{1/2}$ can further split into two other peaks by each. The deconvoluted peak of Mn $3p_{3/2}$ at 641.2 eV and 642.6 eV

(Mn $2p_{1/2}$ at 653 and 655 eV) represents the Mn^{3+} as well as Mn^{4+}, respectively [29]. This data is confirming the Mn present in both +3 and +4 oxidation states.

Fig. 6.4(b) presents the XPS spectrum in Nb 3d core levels for CCTNO ceramic sintered at 1050°C for 8 h. The highest peak at 202.7 and 202.8 eV of Nb $3d_{5/2}$ (Nb $3d_{3/2}$ at 210.2 eV) represents the Nb^{2+}, Nb^{4+} and Nb^{5+}, respectively. Fig. 4(c) shows the XPS spectrum of W 4f core levels for CCTWO at 1100°C for 8h. The main peak 34.9 and 35.2 eV of W $4f_{7/2}$ (W $4f_{5/2}$ at 37.1 and 37.4) represents the W^{4+} and W^{6+}, respectively [30]. The results of Fig 4(b & c) confirmed the oxidation state niobium and tungsten, respectively.

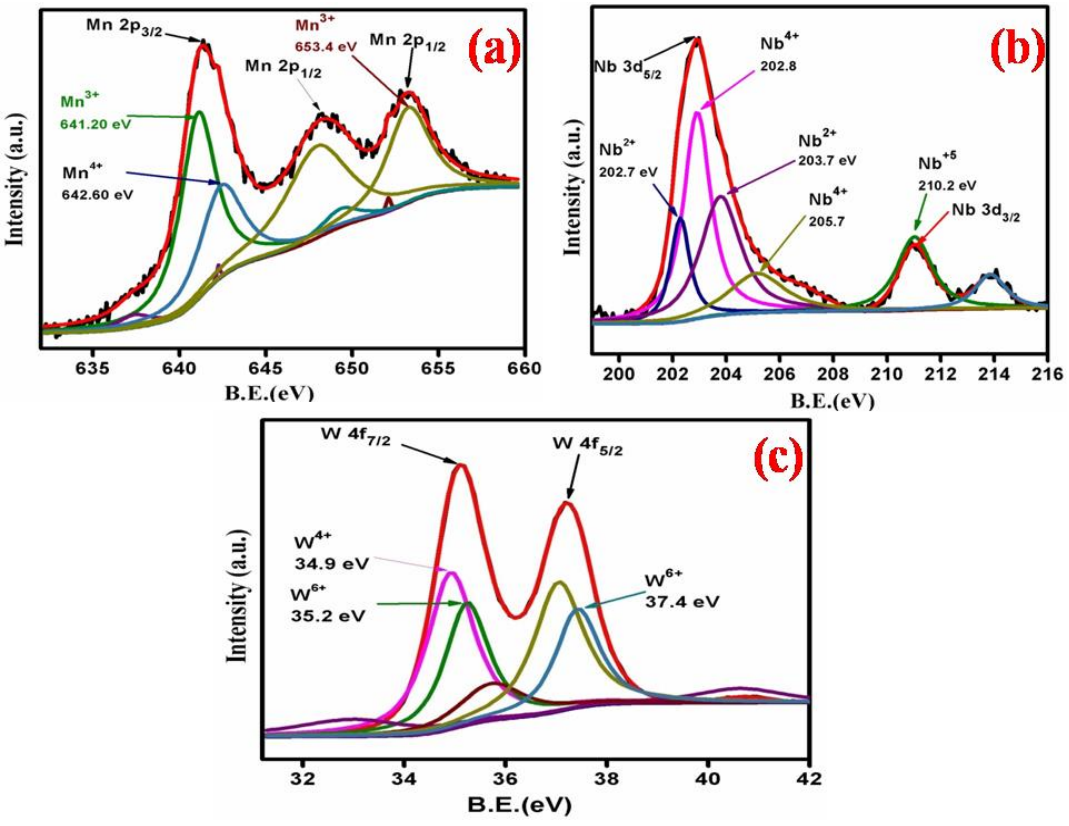

Fig. 6.4. X-ray photo emission spectroscopy (a) Mn 2p, (b) Nb 3d, (c) W 4f, for CCTXO (X= Mn, Nb, W) sintered at 1223 K, 1323 K and 1373 K, respectively for 8 h.

6.3.3 Dielectric studies

In dielectric studies, The CCTO's dielectic function value will be given to compare metal effect. Fig. 6.5(a), 6.6(a), and 6.7(a) illustrate the frequency against dielectric function (εr) at a few selected temperatures of CCTMO, CCTNO, and CCTWO, respectively. The dielectric function (εr) decreases with increasing temperature [6, 25]. The declining behavior of the dielectric function is explained by the Maxwell Wagner equation [2, 26]. In this present work, the dielectric function of both fine and abnormal grain sizes of CCTMO, CCTNO and CCTWO present the dependent frequency in the range of 100 Hz to 1 MHz The abnormal grains size of Mn, Nb and W doped-CCTO produced fine grains (show in fig.6.3 (a-c)) [27, 28]. The dielectric function (εr) of CCTMO, CCTNO, and CCTWO were found to be 800, 600, and 1500 at room temperature (308 K). The dielectric function is occurring to decrease with increasing frequency. Some literature [28] confirms the Nb-doped dielectric function is greater than CCTO. So, all this dopant can be used for refining the dielectrical behavior of CCTO. Many researchers have been investigated that the dielectric constant of the lesser substituted of a metal ion is higher in comparison to a higher substitute of metal ion CCTO [21-27, 28]. Fig. 6.5(b), 6.6(b) and 6.7(b) show the variation dielectric loss (tan δ) from 100 Hz to 1 MHz of CCTMO, CCTNO, and CCTWO at 35^{o}C. At a higher frequency region, the tangent loss decreases in all doped metal ion in CCTO. At higher frequency, the tangent loss of CCTMO, CCTNO, and CCTWO was found to be less than 1 at all selected temperature. The introduction of the doped metal ion in CCTO can exponentially decrease the dielectric constant 3 to 0.5. The result confirms that important role to decreases in dielectric loss of CCTO.

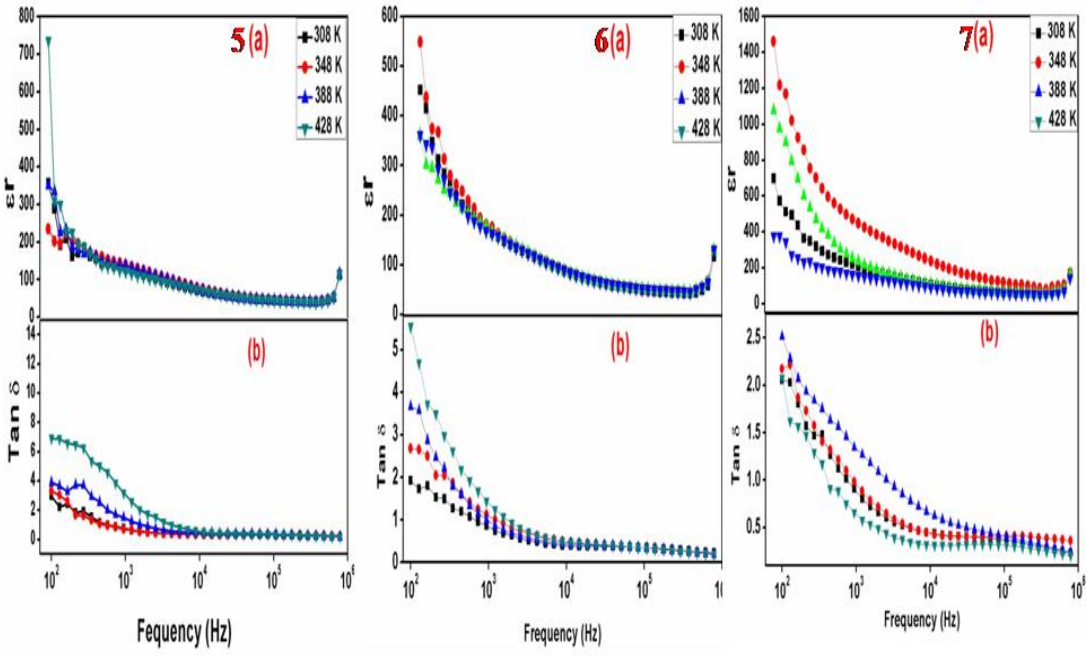

Fig. 6.5(a). Dielectric constant (b) dielectric loss dependent on the frequency at a few selected temperatures of CCTMO sintered at 1223 K for 8h.

Fig. 6.6(a). Dielectric constant (b) dielectric loss dependent on the frequency at a few selected temperatures of CCTNO sintered at 1323 K for 8h.

Fig. 6.7(a). Dielectric constant (b) dielectric loss dependent of frequency at a few selected temperatures of CCTWO sintered at 1373 K for 8h.

Conclusion

In this present work, the influence of microstructure and dielectric function of Mn, Nb, and W doped $CaCu_3Ti_4O_{12}$ (CCTO). The metal doped $CaCu_3Ti_4O_{12}$ is successfully synthesized by a semi-wet method using Metal nitrates, WO_2, Nb_2O_5 and TiO_2 in a stoichiometric amount in molar ratio as starting materials. The phase formation of CCTXO is confirmed by X-ray diffraction pattern sintered at different temperatures and indicates the presence of CCTO as the main phase containing minor phases of TiO_2.

The average crystallite size of CCTMO, CCTWO, and CCTNO was calculated 37.87 ± 10 nm, 56.23 ± 10 nm, and 42.41 ± 10 nm by XRD. The particle size of CCTXO (x= Mn, Nb, and W) occurred to be 44 nm, 101 nm, and 51 nm. The dielectric behaviors are directly affected by dopant metal ion in CCTO samples. The dielectric constant is directly dependent on grain size.

[1] Wang, T., Jin, L., Li, C., Hu, Q., & Wei, X. (2015). Relaxor ferroelectric $BaTiO_3$–$Bi(Mg_{2/3}Nb_{1/3})O_3$ ceramics for energy storage application. *Journal of the American Ceramic Society*, **98**(2), 559-566.

[2] Pandey, S., Kumar, A., Singh, N. B., & Mandal, K. D. (2020). Studies on dielectric and magnetic properties of $CaCu_3Ti_3MnO_{12}$ ceramic synthesized via semi-wet route. *Journal of the Australian Ceramic Society*, **56**(3), 915-922.

[3] Singh, L., Rai, U. S., Mandal, K. D., & Singh, N. B. (2014). Progress in the growth of $CaCu_3Ti_3MnO_{12}$ and related functional dielectric perovskites. *Progress in crystal growth and characterization of Materials*, **60**(2), 15-62.

[4] Zheng, Q., Fan, H., & Long, C. (2012). Microstructures and electrical responses of pure and chromium-doped $CaCu_3Ti_3MnO_{12}$ ceramics. *Journal of alloys and compounds*, **511**(1), 90-94.

[5] De la Rubia, M. A., Leret, P., Del Campo, A., Alonso, R. E., López-Garcia, A. R., Fernández, J. F., & De Frutos, J. (2012). Dielectric behaviour of Hf-doped $CaCu_3Ti_3MnO_{12}$ ceramics obtained by conventional synthesis and reactive sintering. *Journal of the European Ceramic Society*, **32**(8), 1691-1699.

[6] Thongbai, P., Jumpatam, J., Yamwong, T., & Maensiri, S. (2012). Effects of Ta^{5+} doping on microstructure evolution, dielectric properties and electrical response in $CaCu_3Ti_3MnO_{12}$ ceramics. *Journal of the European Ceramic Society*, **32**(10), 2423-2430.

[7] Liu, Y., Chen, Q., & Zhao, X. (2014). Dielectric response of Sb-doped $CaCu_3Ti_3MnO_{12}$ ceramics. *Journal of Materials Science: Materials in Electronics*, **25**(3), 1547-1552.

[8] Sulaiman, M. A., Hutagalung, S. D., Ain, M. F., & Ahmad, Z. A. (2010). Dielectric properties of Nb-doped $CaCu_3Ti_3MnO_{12}$ electroceramics measured at high frequencies. *Journal of alloys and compounds*, **493**(1-2), 486-492.

[9] Barbier, B., Combettes, C., Guillemet-Fritsch, S., Chartier, T., Rossignol, F., Rumeau, A., & Dutarde, E. (2009). $CaCu_3Ti_3MnO_{12}$ ceramics from co-precipitation method: Dielectric properties of pellets and thick films. *Journal of the European Ceramic Society*, **29**(4), 731-735.

[10] Masingboon, C., Thongbai, P., Maensiri, S., Yamwong, T., & Seraphin, S. (2008). Synthesis and giant dielectric behavior of $CaCu_3Ti_3MnO_{12}$ ceramics prepared by polymerized complex method. *Materials Chemistry and Physics*, **109**(2-3), 262-270.

[11] Singh, L., Rai, U. S., Rai, A. K., & Mandal, K. D. (2013). Sintering effects on dielectric properties of Zn-doped $CaCu_3Ti_3MnO_{12}$ ceramic synthesized by modified sol-gel route. *Electronic Materials Letters*, **9**(1), 107-113.

[12] Mu, C., Zhang, H., He, Y., Shen, J., & Liu, P. (2009). Influence of dc bias on the dielectric relaxation in Fe-substituted $CaCu_3Ti_3MnO_{12}$ ceramics: grain boundary and surface effects. *Journal of Physics D: Applied Physics*, **42**(17), 175410.

[13] Senda, S., Rhouma, S., Torkani, E., Megriche, A., & Autret, C. (2017). Effect of nickel substitution on electrical and microstructural properties of $CaCu_3Ti_3MnO_{12}$ ceramic. *Journal of Alloys and Compounds*, **698**, 152-158.

[14] Thongbai, P., Jumpatam, J., Yamwong, T., & Maensiri, S. (2012). Effects of Ta^{5+} doping on microstructure evolution, dielectric properties and electrical response in $CaCu_3Ti_3MnO_{12}$ ceramics. *Journal of the European Ceramic Society*, **32**(10), 2423-2430.

[15] Rai, A. K., Singh, N. K., Acharya, S. K., Singh, L., & Mandal, K. D. (2012). Effect of tantalum substitutions on microstructures and dielectric properties of calcium copper titanate ($CaCu_3Ti_3MnO_{12}$) ceramic. *Materials Science and Engineering: B*, **177**(14), 1213-1218.

[16] Lin, Y. H., Deng, W., Xu, W., Liu, Y., Chen, D., Zhang, X., & Nan, C. W. (2012). Abnormal dielectric behaviors in Mn-doped $CaCu_3Ti_3MnO_{12}$ ceramics and their response mechanism. *Materials Science and Engineering: B*, **177**(20), 1773-1776.

[17] Cai, J., Lin, Y. H., Cheng, B., Nan, C. W., He, J., Wu, Y., & Chen, X. (2007). Dielectric and nonlinear electrical behaviors observed in Mn-doped $CaCu_3Ti_3MnO_{12}$ ceramic. *Applied Physics Letters*, **91**(25), 252905.

[18] Pandey, S., & Mandal, K. D. (2019). Investigation of microstructure, ferroelectric and dielectric behavior of $CaCu_3Ti_{(4-x)}Mn_xO_{12}$ perovskites synthesized through semi-wet route. *SN Applied Sciences*, **1**(12), 1-7.

[19] Lin, Y. H., Cai, J., Li, M., Nan, C. W., & He, J. (2006). High dielectric and nonlinear electrical behaviors in Ti O 2-rich $CaCu_3Ti_3MnO_{12}$ ceramics. *Applied Physics Letters*, **88**(17), 172902.

[20] Mandal, K. D., Rai, A. K., Kumar, D., & Parkash, O. (2009). Dielectric properties of the $Ca_{1-x}LaxCu_3Ti_{4-x}Co_xO_{12}$ system (x= 0.10, 0.20 and 0.30) synthesized by semi-wet route. *Journal of alloys and compounds*, **478**(1-2), 771-776.

[21] Singh, L., Sin, B. C., Kim, I. W., Mandal, K. D., Chung, H., & Lee, Y. (2016). A novel one-step flame synthesis method for tungsten-doped CCTO. *Journal of the American Ceramic Society*, **99**(1), 27-34.

[22] Sulaiman, M. A., Hutagalung, S. D., Ain, M. F., & Ahmad, Z. A. (2010). Dielectric properties of Nb-doped $CaCu_3Ti_3MnO_{12}$ electroceramics measured at high frequencies. *Journal of alloys and compounds*, **493**(1-2), 486-492.

[23] Zheng, Q., Fan, H., & Long, C. (2012). Microstructures and electrical responses of pure and chromium-doped $CaCu_3Ti_3MnO_{12}$ ceramics. *Journal of alloys and compounds*, **511**(1), 90-94.

[24] Senda, S., Rhouma, S., Torkani, E., Megriche, A., & Autret, C. (2017). Effect of nickel substitution on electrical and microstructural properties of $CaCu_3Ti_3MnO_{12}$ ceramic. *Journal of Alloys and Compounds*, **698**, 152-158.

[25] Thongbai, P., Jumpatam, J., Putasaeng, B., Yamwong, T., & Maensiri, S. (2012). The origin of giant dielectric relaxation and electrical responses of grains and grain boundaries of W-doped $CaCu_3Ti_3MnO_{12}$ ceramics. *Journal of Applied Physics*, **112**(11), 114115.

[26] George, M., Nair, S. S., Malini, K. A., Joy, P. A., & Anantharaman, M. R. (2007). Finite size effects on the electrical properties of sol–gel synthesized $CoFe_2O_4$ powders: deviation from Maxwell–Wagner theory and evidence of surface polarization effects. *Journal of Physics D: Applied Physics*, **40**(6), 1593.

[27] Sulaiman, M. A., Hutagalung, S. D., Mohamed, J. J., Ahmad, Z. A., Ain, M. F., & Ismail, B. (2011). High frequency response to the impedance complex properties of Nb-doped $CaCu_3Ti_3MnO_{12}$ electroceramics. *Journal of Alloys and Compounds*, **509**(18), 5701-5707.

[28] Sulaiman, M. A., Hutagalung, S. D., Ain, M. F., & Ahmad, Z. A. (2010). Dielectric properties of Nb-doped $CaCu_3Ti_3MnO_{12}$ electroceramics measured at high frequencies. *Journal of alloys and compounds*, **493**(1-2), 486-492.

[29] Sannigrahi, J., Chattopadhyay, S., Dutta, D., Giri, S., & Majumdar, S. (2013). Magnetic and electric properties of $CaMn_7O_{12}$ based multiferroic compounds: effect of electron doping. *Journal of Physics: Condensed Matter*, **25**(24), 246001.

[30] Singh, L., Sin, B. C., Kim, I. W., Mandal, K. D., Chung, H., & Lee, Y. (2016). A novel one-step flame synthesis method for tungsten-doped CCTO. *Journal of the American Ceramic Society*, **99**(1), 27-34.

[31] Pandey, S., Kumar, V., & Mandal, K. D. (2020). Studies of sintering temperature on the microstructure, magnetic and dielectric behavior of $CaCu_3Ti_{3.5}Mn_{0.5}O_{12}$ ceramic synthesized by semi-wet route. *SN Applied Sciences*, **2**(3), 1-9.

Summary

- $CaCu_3Ti_4O_{12}$ (CCTO) ceramic was synthesized by semi-wet route at low temperature and single phase formation was confirmed by XRD studies.
- The elemental compositions of Mn-doped CCTO ceramics obtained by EDX data were fit as per stoichiometric ratio of the elements in both the ceramics.
- Dielectric constant of Mn-doped CCTO ceramic was found lower than CCTO ceramic at all measured temperature and frequency.
- The blocking temperature of CCTO and doped CCTO ceramics obtained by magnetic measurement was found to be 25 K and 155 K, respectively.
- The dielectric constant of Mn-doped composites were found to be 100 to 1200 at 303, 363, and 423 K and 484 K, at 100 Hz. the dielectric constant is highest in the case of low concentration of Mn doped CCTO.
- The Neel's temperature obtained by magnetic measurement was found to be 25 K for all the synthesized composite.

Future Scope

In general, this work has been important for nature. The everyday increasing demand for various applications, semiconducting technology sustain blest in its drive for high transistor densities and faster transistor.

Ceramic has inorganic and non-metallic materials constituted from metal and a non metal compounds. New days ceramic materials have enormously expanded many possible applications. Most of the new materials have used in our daily life. There is now a strong researcher effort to discover the new ceramics and their composites for various applications. Composite have played an important role in industrial application. Composites have constituted penetration into devices end-use segments and the development efforts newer composition for existing and novel application.

- The calcium copper titanium oxides ($C_aCu_3Ti_4O_{12}$) may be used in various applications because of its high dielectric constant and low coercivity value.
- The $CaCu_3Ti_3MnO_{12}$ ceramics shows great interested in ferroelectric materials for its application in non-volatile random access memories (NRAM) and advanced MOS transistors.
- The composite materials of CCTO and BCTO shows enhanced properties as compared to its parents components and may be used in capacitors, microelectronic devices and electronic chips, transistors.
- The composite materials show soft as well as hard magnetic nature due to different composition of parent compound which are suitable for computer chips, transformer, hard disk and floppy disk.
- The properties of ceramics and composite largely depend on the synthesis route, sintering duration and sintering temperature. In future, these composite may be

studied by changing the synthesis route and sintering condition.

- The internal properties of the composite may be studied by impedance analysis to see the electrical and dielectrical properties of grain and grain boundries.
- Electrical polarization of the composite may be studied with variation of temperature by P-E loop tracer.